The electrochemical reduction of dioxygen and hydrogen peroxide by molecular copper catalysts
Langerman, M.

Chapter 3

Mechanistic study of the activation and the electrocatalytic reduction of hydrogen peroxide by Cu-tmpa in neutral aqueous solution

Hydrogen peroxide plays an important role as an intermediate and product in the reduction of dioxygen by copper enzymes and mononuclear copper complexes. The copper(II) tris(2-pyridylmethyl)amine complex (Cu-tmpa) has been shown to produce H_2O_2 as an intermediate during the electrochemical 4-electron reduction of O_2. We investigated the electrochemical hydrogen peroxide reduction reaction (HPRR) by Cu-tmpa in a neutral aqueous solution. The catalytic rate constant of the reaction was shown to be one order of magnitude lower than the reduction of dioxygen. A significant solvent kinetic isotope effect (KIE) of 1.4 to 1.7 was determined for the reduction of H_2O_2, pointing to a Fenton-like reaction pathway as the likely catalytic mechanism, involving a single copper site that produces an intermediate copper(II) hydroxyl species and a free hydroxyl radical anion in the process.

3.1. Introduction

The formation, decomposition, and reduction of H_2O_2 plays an important role in many (bio)chemical processes, such as oxidation reactions,[1-4] fuel cell chemistry,[5-8] and enzymatic reactions. Many peroxidases and catalases scavenge and disproportionate H_2O_2 into O_2 and H_2O to prevent formation of reactive oxygen species (ROS) that induce damage to their hosts.[9-10] In the context of elucidating the oxidative catalytic reactions taking place at the active sites of these enzymes, often containing copper, iron, or manganese ions, many synthetic mimic catalysts have been synthesized and studied intensively.[11-15]

Of particular interest are lytic polysaccharide monooxygenases (LPMOs), a family of copper-containing enzymes that are able to degrade lignocellulosic biomass.[16-20] Over the last decade, since the discovery of the LPMO family of enzymes, significant scientific effort has been put into the determination of the structure and active site of LPMOs. It was revealed that all LPMOs contain a type II copper centre as their active site in a Cu^{II} resting state, with little variation in the primary coordination sphere for the different LPMOs.[18, 21] The primary coordination sphere is formed by the coordination of three N ligands in a T-shaped geometry around the copper centre, with the whole primary coordination sphere conforming to either a tetrahedral or trigonal-bipyramidal geometry. The N ligands comprise a monodentate histidine and a bidentate histidine, coordinating with both the imidazole and backbone nitrogen coordinating to the copper centre, the so-called histidine brace. Polysaccharides are cleaved by LPMOs through an oxidative mechanism, and it was shown that both O_2 and H_2O_2 can act as the oxidant. Additionally, in the absence of polysaccharide substrate, H_2O_2 is produced by the enzyme in the presence of O_2. This behaviour shows similarities to that of Cu-tmpa (tmpa = tris(2-pyridylmethyl)amine), which can both reduce O_2 and H_2O_2, while also producing H_2O_2 as a detectable intermediate during the catalytic cycle. Density functional theory (DFT) calculations of LPMO systems have shown that the most likely catalytic species responsible for the cleavage of polysaccharides is a copper oxyl radical (Cu^{II}-$O^{•-}$) species. Several different routes have been suggested for the catalytic pathway.[22] Fenton chemistry plays an important role in many of these processes, and it has been shown that Fenton-like reactions can take place between Cu^{I} complexes and H_2O_2, resulting in the homolytic cleavage of the O-O bond.[23-24]

Another enzyme that shows similarities to both the LPMOs and Cu-tmpa, is the particulate methane monooxygenase (pMMO), which activates and reduces dioxygen in order to oxidize methane to methanol. Many conflicting suggestions have been proposed on the nature of the Cu_B active site in pMMO, which was either considered a mononuclear or dinuclear copper centre,[21, 25-29] but recent experimental work points towards a catalytic centre containing a mononuclear copper ion in a square pyramidal

geometry and includes a histidine brace similar to the LPMOs.[30]

How hydrogen peroxide is formed and activated is a very important research question, taking into account potential applications of this chemistry. In traditional polymer electrolyte membrane (PEM) fuel cells, formation of H_2O_2 is considered undesirable as it leads to both catalyst poisoning and damaging of the proton exchange membrane.[5, 31-34] However, more recently hydrogen peroxide has also been suggested as an alternative sustainable fuel or oxidant in fuel cells, owing to the broad range of standard equilibrium potentials associated with H_2O_2.[8, 35-38] Currently, the bulk of H_2O_2 is synthesized through the anthraquinone process, which uses several different catalysts (Pd or Ni), creates significant amount of waste products, and requires expensive separation steps in order to obtain concentrated H_2O_2.[39] As such, despite the use of H_2O_2 as a sustainable oxidant in many chemical reaction, it's production is not sustainable.[3, 40] Indeed, electrochemical synthesis by selective 2-electron reduction of O_2 at low overpotentials would be a more desirable approach to obtain H_2O_2.

Understanding how hydrogen peroxide is activated and reduced at copper sites and what drives the 4-electron versus the 2-electron selectivity for the reduction of O_2 by copper catalysts is essential for the design of of new catalysts for the oxygen reduction reaction, and the electrochemical production of H_2O_2. Here, we report our findings on the electrocatalytic behaviour of Cu-tmpa towards the hydrogen peroxide reduction reaction (HPRR) under neutral aqueous conditions, resulting in solvent kinetic isotope effects (KIE), rate orders, and catalytic rate constants. Based on this, we propose a catalytic mechanism for the Cu-tmpa catalysed HPRR.

3.2. Results and discussion

3.2.1. Electrocatalytic reduction of hydrogen peroxide by Cu-tmpa

The electrochemical behaviour of Cu-tmpa towards the ORR was extensively discussed in the previous chapter, where it was shown that the reduction of H_2O_2 to H_2O is an essential part of the catalytic cycle to achieve the four-electron reduction of O_2 to H_2O. Thus, the electrocatalytic reduction of H_2O_2 by Cu-tmpa in a phosphate buffer (PB) solution of pH 7, containing 100 mM phosphate salts (NaH_2PO_4 and Na_2HPO_4), was investigated in detail and the results are discussed in this chapter. In Figure 3.1a, a CV measured in the aforementioned solution in the presence of 1.1 mM H_2O_2 shows a peak-shaped catalytic wave. The catalytic half-wave potential ($E_{cat/2}$) of this catalytic wave is situated at 0.34 V vs. RHE, which is close to the values for the ORR of 0.31 V (Chapter 2) to 0.33 V (this work) vs. RHE observed under stationary conditions. For both the HPRR and the ORR a catalytic peak potential of 0.26 V was found. Additionally, a
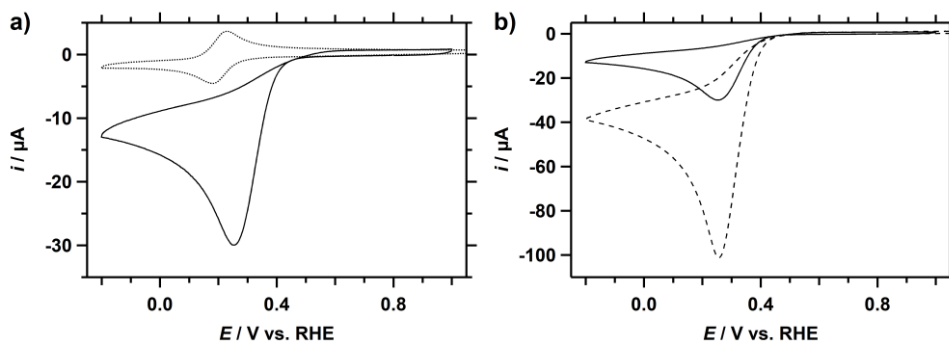
Figure 3.1 a) CVs of Cu-tmpa (0.30 mM) in the presence of 1 atm Ar (dotted) or 1.1 mM H_2O_2 (solid). $E_{cat/2}$ = 0.34 V vs. RHE. **b)** Comparison of CVs of 1.1 mM H_2O_2 (solid) and 1 atm O_2 (dashed) reduction by Cu-tmpa (0.30 mM). Conditions: pH 7 PB ([PO_4] = 100 mM), 293 K, 100 mV s^{-1} scan rate, 0.0707 cm^2 electrode surface area.

comparison of the CVs of the electrochemical reduction of H_2O_2 and O_2 reveals that the peak catalytic current (i_{cat}) for the HPRR (30 µA) is less than a third of that of ORR (100 µA), as shown in Figure 3.1b. While a lower i_{cat} can be an indication of a slower catalytic reaction, this only holds true if the substrate and catalytic mechanism are the same when comparing between CV measurements. This is clearly not the case for the ORR and HPRR, and the large difference in peak catalytic current can be explained by the difference in catalytic electron transfer number n of the reaction and the diffusion coefficient D of the substrate. Thus, considering the different electron transfer number for the ORR (n = 4) and the HPRR (n = 2), a D_{O2} of 2×10^{-5} cm^2 s^{-1}, and a D_{H2O2} of 0.6–1.4×10^{-5} cm^2 s^{-1},[41-42] an expected ratio between the respective peak catalytic currents ($i_{cat,H2O2}/i_{cat,O2}$) can be determined. If the HPRR is limited in H_2O_2 concentration, as was the case for O_2 during the ORR for this catalyst, and i_{cat} is therefore not determined by the catalytic rate constant or catalyst concentration, a $i_{cat,H2O2}/i_{cat,O2}$ ratio in the range of 0.27 to 0.42 is expected. The $i_{cat,H2O2}/i_{cat,O2}$ derived from the CVs in Figure 3.1b falls within the calculated ratio, indicating that the HPRR is also limited in substrate concentration at 1.1 mM H_2O_2 and a Cu-tmpa concentration of 0.3 mM.

3.2.2. Catalyst concentration dependence

The relationship between the catalytic current and the catalyst concentration was investigated by determining the peak catalytic current at a low catalyst concentration range (1.0–2.5 µM), in the presence of 1.1 mM H_2O_2. While the GC electrode showed no activity towards the reduction of H_2O_2, background correction was applied to the CV to remove contributions in the range of 0.5 to 1 µA from the GC double layer. The resulting linear sweep voltammograms (LSV) are shown in Figure 3.2a. For each Cu-tmpa concentration, the peak current is visible around 0.23 V vs. RHE, with an $E_{cat/2}$ at
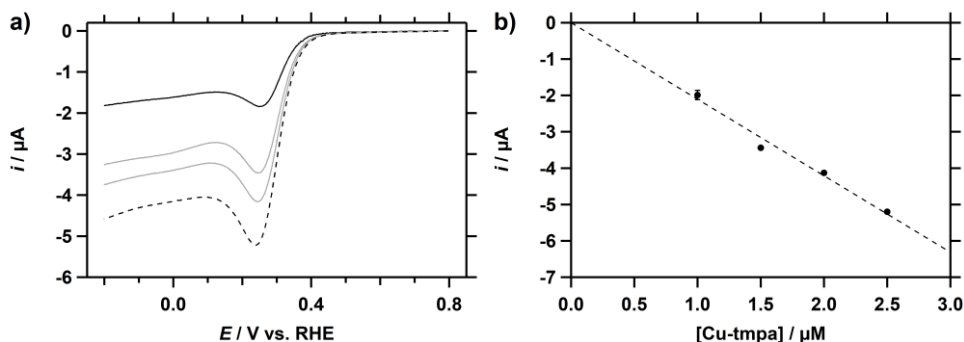
Figure 3.2 a) Background corrected linear sweep voltammograms (LSV) of the reduction of H_2O_2 (1.1 mM) for different concentrations of Cu-tmpa; 1.0 (solid black)/1.5/2.0/2.5 (dashed) μM. **b)** The peak catalytic current i_{cat} taken at 0.23 V vs. RHE plotted against the catalyst concentration. Conditions: pH 7 PB ([PO_4] = 100 mM), 293 K, 100 mV s^{-1} scan rate.

0.31 V. Both potentials have shifted closer to the redox potential of the catalyst compared to the E_{cat} and $E_{cat/2}$ observed at high catalyst concentration, which is expected when substrate diffusion limitations play a lesser role during catalysis. For the HPRR, a linear relationship is observed between the i_{cat} and the Cu-tmpa concentration (Figure 3.2b), as was also shown for the Cu-tmpa catalysed ORR. A plot of log(i_{cat}) as a function of the logarithm of the catalyst concentration has a slope of 1.05 (R^2 = 0.96), confirming the first-order nature of the catalytic reaction (Figure B.1). Additionally, the same experiment performed at higher H_2O_2 concentration of 10 mM over a Cu-tmpa concentration range from 1 to 10 μM showed the same first-order dependence in catalyst concentration (see Figure B.2).

3.2.3. Relationship between hydrogen peroxide concentration and catalytic activity.

As opposed to O_2, it is far more straightforward to increase the concentration of H_2O_2 in the solution to study the relationship between the substrate concentration and the catalytic reaction. CVs were measured in a PB pH 7 electrolyte solution containing Cu-tmpa and different H_2O_2 concentrations ranging from 1.1 to 30 mM. These CVs show the familiar peak shaped catalytic wave around 0.25 V vs. RHE (Figure 3.3a), but from a H_2O_2 concentration of 20 mM and upwards a shoulder or second reduction event appears below 0.1 V in the CV, and becomes clearly visible at 30 mM. Expanding the concentration range to 100 mM shows that the peak current of this second catalytic wave keeps increasing with the increasing H_2O_2 concentration, while the peak current of the first catalytic stays the same. Moreover, the potential at which the peak catalytic current of this reduction is reached also shifts more negatively with increasing concentration. Another observation is that an oxidation event appears in the positive
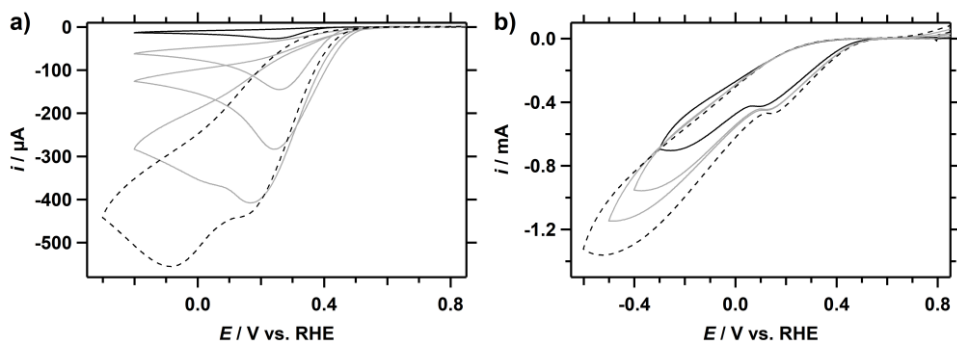
Figure 3.3. CVs of the reduction of H_2O_2 in the presence of 0.3 mM Cu-tmpa for a range of H_2O_2 concentrations under 1 atm Ar; **a)** 1.1 (solid black)/5.0/10/20/30 (dashed) mM, **b)** 40 (solid black)/60/80/100 (dashed) mM. Conditions: pH 7 PB ([PO$_4$] = 100 mM), 293 K, 100 mV s^{-1} scan rate.

potential window above 0.6 V vs. RHE at H_2O_2 concentrations of 40 mM and higher (Figure B.3a). Although this oxidation could be the result of scanning to a lower potential, both the 30 and 40 mM H_2O_2 measurements have the same potential window, yet this oxidation is only present in the CVs corresponding to the solution containing 40 mM H_2O_2 and higher. Therefore, it is more likely that the observed oxidation is related to the increased peroxide concentration. The onset of this catalytic oxidation is close to the standard reduction potential for the oxidation of H_2O_2 to O_2 (E^0 = 0.695 V vs. RHE), making the 2-electron oxidation of H_2O_2 the most likely candidate for the observed H_2O_2-concentration dependent oxidation. The GC electrode is not able to activate H_2O_2 in neutral solution at these low potentials, as it was only shown to catalyse the oxidation above 1.4 V vs. RHE in a PB pH 7.4 buffer (though at 1.0 mM H_2O_2),[43] while under basic conditions (> pH 10) oxidation was observed above 0.9 V vs. RHE while rotating (250 mM H_2O_2).[44] To confirm this, CVs were measured with a GC electrode in a PB pH 7 electrolyte solutions containing H_2O_2 concentrations ranging from 1.5 to 500 mM (Figure B.3b). No anodic currents were observed in the absence of Cu-tmpa, showing the involvement of the copper complex in apparent oxidation of H_2O_2.

A plot of the peak catalytic current i_{cat} derived from the obtained CVs versus the H_2O_2 concentration, reveals two different regimes where reduction of hydrogen peroxide takes place (Figure 3.4a). A linear relationship between i_{cat} and the concentration is apparent at low concentrations of H_2O_2, but above 30 mM the catalytic current of the first reductive wave is no longer dependent on the substrate concentration. When the second catalytic wave at lower potential is considered, it clearly shows that the corresponding $i_{cat,2}$ still has a mostly linear dependency on H_2O_2 concentration (Figure 3.4b), although a slight deviation from an ideal linear relationship
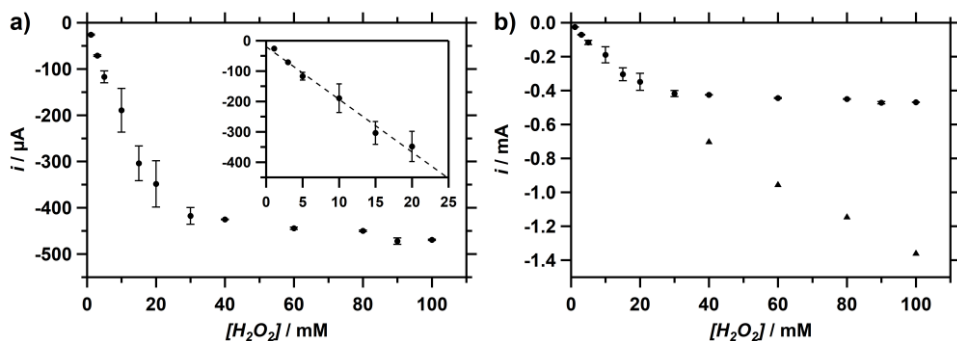
Figure 3.4. a) Catalytic current as a function of H_2O_2 concentration in the presence of 0.3 mM Cu-tmpa, showing a $[H_2O_2]$ dependent (zoom in inset) and independent regime. **b)** An expanded view including the i_{cat} values of the 2nd catalytic reduction (triangles). Conditions: pH 7 PB ($[PO_4]$ = 100 mM), 293 K, 100 mV s^{-1} scan rate.

is visible at higher concentrations. These results show that the reduction reaction of H_2O_2 to water is both first-order in H_2O_2 and Cu-tmpa.

The existence of two distinct catalytic waves can be related to the buffer capacity of the electrolyte solution at pH 7. As the hydrogen peroxide concentration is approaching that of phosphate buffer in the electrolyte solution at these higher concentrations, the buffering ability of the solution can become compromised. This would result in significantly increased pH gradient close to the electrode surface. Thus, the appearance of a second catalytic reduction at a lower potential is likely the result of a shift in proton source for the reduction of H_2O_2 to H_2O, possibly from H_2O or even H_2O_2 itself, as the pK_a of hydrogen peroxide is 11.75 in water.

3.2.4. Kinetic isotope effect studies of the peroxide reduction reaction

To get more insight into the rate-determining step in the mechanism of the electrocatalytic reduction of H_2O_2, solvent kinetic isotope effects (KIE) were determined. Cyclic voltammograms were measured in a 0.1 M phosphate buffer (pH 7) solution containing 0.3 mM Cu-tmpa. Both deuterated and non-deuterated phosphate buffers contained the same concentration and ratio of phosphate salts (0.1 M). The pH*, defined as the apparent pH directly determined from a H_2O calibrated pH meter in a D_2O solution, of the deuterated solution was determined to be 7.13. Using Eq. 3.1 to convert the pH* to the pH,[45] this pH* value corresponds to a pH of 7.03. This agrees well with the pH of 7.01 that was measured for the non-deuterated electrolyte solution. The pD can in turn be calculated using Eq. 3.2, resulting in a pD of 7.58.

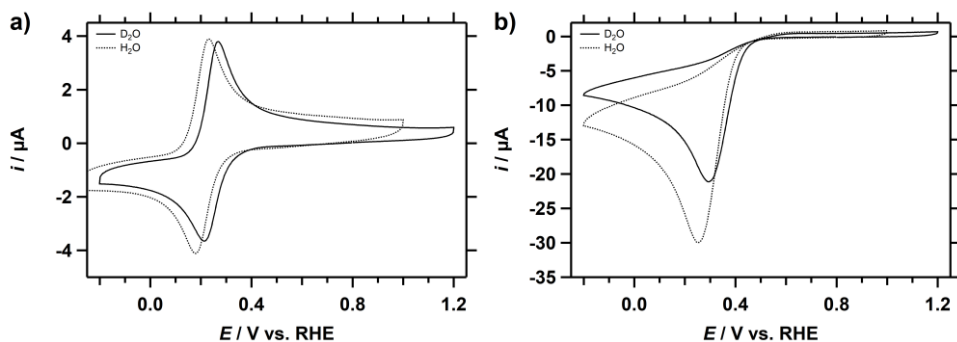$$pH = 0.929 \times pH^* + 0.41 \tag{3.1}$$

$$pD = pH^* + 0.45 \tag{3.2}$$

45

Figure 3.5. a) CVs of 0.3 mM Cu-tmpa under 1 atm Ar in a deuterated (solid) and non-deuterated (dotted) PB electrolyte solution. b) CVs of the catalytic reduction of H_2O_2 (1.1 mM under 1 atm Ar) by Cu-tmpa in a deuterated (solid) and non-deuterated (dotted) PB electrolyte solution. Conditions: pH 7 PB ([PO_4] = 100 mM), 293 K, 100 mV s^{-1} scan rate.

In the presence of 1 atm argon, and in the absence of hydrogen peroxide, the $E_{1/2}$ of the Cu-tmpa redox couple is positively shifted by 37 mV in the deuterated phosphate buffer compared to the non-deuterated phosphate buffer (Figure 3.5a). Saturating the deuterated electrolyte solution in the RHE compartment with H_2 instead of D_2 is the likely cause of this, the observed potential shift being similar to the difference in equilibrium potential E° for the H^+/H_2 and D^+/D_2 couples.[46-47] Upon the addition of 1.1 mM H_2O_2 to the electrolyte solutions, a clear difference in catalytic rates can be observed between the deuterated and non-deuterated electrolyte solutions (Figure 3.5b). As with the redox couple in the absence of substrate, the $E_{cat/2}$ of the catalytic wave is positively shifted by 37 mV in the deuterated solution. More striking is the decrease of the peak catalytic current i_{cat} in the deuterated solution, from 30 to 20 µA.

Conversely, when the catalytic activity of Cu-tmpa towards the ORR in deuterated PB (pH 7) electrolyte solution in the presence of 1 atm O_2 is investigated by cyclic voltammetry (Figure 3.6), the catalytic half-wave potential $E_{cat/2}$ is again shifted positively by 37 mV. The difference of the i_{cat} between the deuterated solution and the non-deuterated solution is only 5 µA, which is insignificant compared to the difference observed for the H_2O_2 reduction. This is in line with the observations that the electrocatalytic ORR by Cu-tmpa is severely rate-limited in the mass-transport of O_2 at a Cu-tmpa concentration of 0.3 mM,[48] and suggests that this is the case in both non-deuterated and deuterated electrolyte solutions.

The KIE is defined as the ratio between the catalytic rate constants in aqueous and deuterated solutions. The electrocatalytic rate constant is directly proportional to the catalytic current enhancement, e.g. the squared ratio of i_{cat} over i_p, where the i_p is the peak reductive current of the Cu$^{II/I}$ redox couple. Thus, the KIE can be determined by applying Eq. 3.3 to the values obtained from the CVs under both conditions.
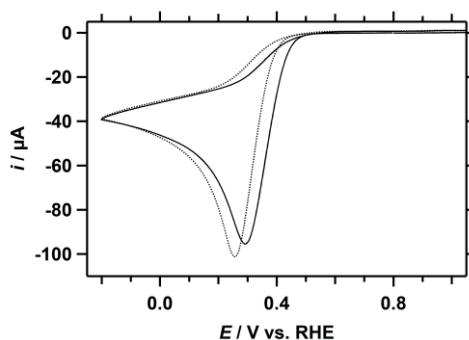
Figure 3.6. CVs of the catalytic reduction of O₂ (1 atm) by Cu-tmpa (0.3 mM) in a deuterated (solid) and non-deuterated (dotted) PB electrolyte solution. Conditions: pH 7 PB ([PO₄] = 100 mM), 293 K, 100 mV s⁻¹ scan rate.

$$KIE = \frac{k_{obs,H}}{k_{obs,D}} \propto \frac{(i_{cat}/i_p)_H^2}{(i_{cat}/i_p)_D^2} \tag{3.3}$$

This resulted in a solvent KIE value of 1.65 for the reduction of hydrogen peroxide, which indicates that breaking of an O–H bond is involved in the rate-determining step of the catalytic reaction. While the determined KIE value is not particularly large, it is in the range of KIEs that are associated with homolytic cleavage of the O-O bond of the Cu^{II}-OOH, in conjunction with a proton transfer.[49-51] However, it was shown in section 3.2.1 and 3.2.3 that the HPRR by Cu-tmpa is mass-transport limited in H_2O_2 under the experimental conditions used here, which may underestimate the KIE obtained from i_{cat} derived from the CVs in Figure 3.5b. Directly deriving the rate constants under non mass-transport limiting conditions, will result in a more accurate determination of the KIE.

3.2.5.   Reaction kinetics and FOWA of the HPRR

While a quick analysis of cyclic voltammograms of the ORR and HPRR by Cu-tmpa (Figure 3.1b) already reveals that HPRR by Cu-tmpa is significantly slower than ORR under the same catalytic conditions and substrate concentrations, the rate constants of the reaction can be determined via foot-of-the-wave analysis (FOWA) or by direct determination using the catalytic current enhancement. Using the FOWA method to determine rate constants, only the beginning of the catalytic wave is used, a region which is not affected by substrate consumption, catalyst deactivation, product inhibition or other side phenomena. In this way the ideal or maximum turnover frequency associated with the catalytic reaction can be determined.[52-55] A detailed description of the FOWA is available in Appendix A.9.

For the FOWA, a CV was measured in triplicate in a PB (pH 7) electrolyte solution

containing 0.3 mM Cu-tmpa and 1.1 mM H_2O_2, using a freshly polished GC electrode. The resulting CVs are shown in Figure B.4a. From these CVs, plots of the current enhancement i_c/i_p vs. $exp[-F/RT\,(E - E_{1/2})]$ were constructed (Figure B.4c). Here, i_c is the current associated with the catalytic HPRR reaction at the applied potential E and i_p is the peak cathodic current associated with the $Cu^{II/I}$ redox couple of Cu-tmpa. In the foot-of-the-wave region, a linear fit (Figure B.4e; $R^2 > 0.98$) was applied between the onset of the HPRR and the potential at which i_c/i_p is at least larger than 1.6, i.e. the potential where the catalytic current is 60% larger than the peak cathodic current of the $Cu^{II/I}$ redox couple. The catalytic onset is defined as $i_c/i_{redox} \geq 2$, where i_{redox} is the current associated with the reduction of the catalyst measured at the applied potential E, in the absence of H_2O_2. From the slope of the linear fit, the TOF_{max} for the HPRR by Cu-tmpa in pH 7 phosphate buffer solution containing 1.1 mM H_2O_2 was determined to be $2.1 \times 10^5 \pm 0.1 \times 10^5$ s^{-1}. This is one order of magnitude (9 times) less than was reported for the ORR in Chapter 2 (Figure 3.7a). Using the same approach, the TOF_{max} for the HPRR in the deuterated pH 7 phosphate buffer solution was determined to be $1.5 \times 10^5 \pm 0.1 \times 10^5$ s^{-1}. A comparison of the TOF_{max} of the HPRR in H_2O and D_2O is shown in Figure 3.7b and confirms that the Cu-tmpa catalysed HPRR is indeed slower in D_2O. By applying Eq. 3.3, where TOF_{max} was used as the k_{obs}, a KIE of 1.37 ± 0.14 was calculated.

$$\frac{i_{cat}}{i_p} = 2.24n\sqrt{\frac{RT}{Fv}k_{obs}} \tag{3.4}$$

$$i_p = 0.446nFSC^0_{cat}\sqrt{\frac{Fv}{RT}D_{cat}} \tag{3.5}$$
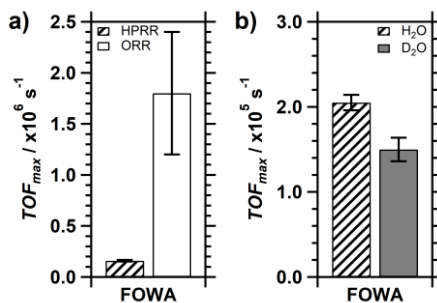

Figure 3.7. a) Comparison between the TOF_{max} of Cu-tmpa for the HPRR (1.1 mM H_2O_2 under 1 atm Ar) and the ORR (1 atm O_2) as determined by FOWA. b) Comparison between the TOF_{max} of the HPRR in H_2O and D_2O. Conditions: pH 7 PB ([PO_4] = 100 mM), 293 K, 100 mV s^{-1} scan rate.
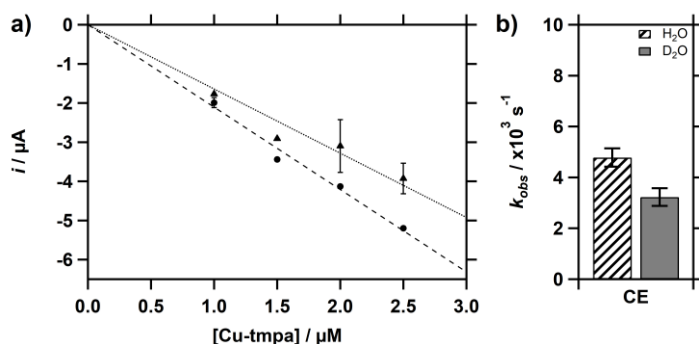
Figure 3.8. a) The peak catalytic current i_{cat} plotted against the Cu-tmpa concentration in a deuterated (triangles) and non-deuterated (circles) PB electrolyte solution containing 1.1 mM H_2O_2 under 1 atm Ar. **b)** Comparison for the k_{obs} derived from the current enhancement (CE) between the hydrogen peroxide reduction in H_2O and D_2O. Conditions: pH 7 PB ([PO_4] = 100 mM), 293 K, 100 mV s^{-1} scan rate.

A more direct approach to obtain a rate constant can be achieved by using the catalytic current enhancement i_{cat}/i_p and applying Eq. 3.4, where R, T and F are known constants, v is the scan rate (V/s), and n is the number of electrons transferred during the catalytic reaction. The current enhancement was determined from the background-corrected peak catalytic current i_{cat} at low catalyst concentration (1.0–2.5 µM) in the presence of 1.1 mM H_2O_2, as discussed in section 3.2.2. No redox current is visible above the double layer current at these low catalyst concentrations. Therefore, for each catalyst concentration the i_p was calculated using the diffusion coefficient of Cu-tmpa (D = 4.9×10^{-6} cm^2 s^{-1}) by applying the Randles-Sevcik equation (Eq. 3.5). This resulted in a k_{obs} of 4.8×10^3 ± 0.4×10^3 s^{-1} (Figure 3.8). Repeating the same experiments in deuterated electrolyte solutions resulted in a k_{obs} of 3.2×10^3 ± 0.4×10^3 s^{-1}. Equation 3.3 was applied to these catalytic rate constants giving a KIE of 1.48 ± 0.17, showing that at both low and high catalyst concentration, and under both substrate limited and non-limiting conditions, a significant kinetic isotope effect is observed.

3.2.6.   Discussion

As demonstrated, the electrocatalytic HPRR by Cu-tmpa is a first-order reaction in both the catalyst and the hydrogen peroxide substrate. Using FOWA, the TOF$_{max}$ for the reduction of H_2O_2 was shown to be one order of magnitude lower than that of the 2-electron reduction of O_2 to H_2O_2, consistent with the analysis of the Tafel slopes for ORR and HPRR reported in Chapter 2. The HPRR k_{obs} (4.8×10^3 s^{-1}) that was determined at low catalyst concentration was significantly lower than the FOWA-derived TOF$_{max}$ (2.1×10^5 s^{-1}) at higher catalyst concentration. Such a k_{obs} < TOF$_{max}$ is expected due to previously mentioned deviations from an ideal catalytic system.

However, the difference between the k_{obs} and the TOF$_{max}$ of the HPRR is significantly

larger (2.5 times) than the difference between the k_{obs} (1.5×10^5 s^{-1}) and TOF$_{max}$ (1.8×10^6 s^{-1}) of the ORR that we have previously reported. A few factors can explain this difference. Firstly, during the ORR the partial 2-electron reduction of O_2 to H_2O_2 and the 2-electron reduction of H_2O_2 both contribute to the peak catalytic current, each with a different catalytic rate. Thus, the intermediate H_2O_2 is generated in situ near the electrode surface, thereby minimizing the effect of mass-transport of H_2O_2 to the electrode on the subsequent 2-electron reduction to H_2O. Given that the diffusion constant of H_2O_2 (0.6–1.4×10^{-5} cm^2 s^{-1}) is significantly lower than that of O_2 (2.0×10^{-5} cm^2 s^{-1}), this would enhance the catalytic current associated with the reduction of H_2O_2, contributing to a higher overall k_{obs} for the 4-electron ORR as determined via the current enhancement (CE) i_{cat}/i_p. This would result in a smaller difference between the k_{obs} and TOF$_{max}$ for the ORR, where the latter is derived from the partial 2-electron reduction of O_2. Conversely, for the HPRR both the FOWA and CE rate constants are associated with the same 2-electron reduction of H_2O_2. During the HPRR diffusion of H_2O_2 to the electrode does play a role and does not benefit of an increased catalytic rate due to in situ generation of the substrate that resulted in a smaller difference between the k_{obs} and TOF$_{max}$ for the ORR.

For the ORR, part of this can be explained by the fact that the full 4-electron reduction takes place at the potential where k_{obs} is determined for the ORR, while for the FOWA only the partial 2-electron ORR was considered. During the 4-electron reduction of O_2, the intermediate H_2O_2 is generated in situ near the electrode surface, thereby minimizing the effect of mass-transport of H_2O_2 to the electrode on the subsequent 2-electron reduction to H_2O. This would enhance the catalytic current associated with the reduction of H_2O_2, contributing to a higher apparent k_{obs} for the 4-electron ORR as determined via current enhancement, as both the partial reduction of O_2 and the reduction of H_2O_2 contribute to the overall catalytic reaction rate. Conversely, for the HPRR both the FOWA and CE rate constants are associated with the same catalytic reaction, specifically the 2-electron reduction of H_2O_2. Thus, a smaller difference between the TOF$_{max}$ and k_{obs} would be observed for the ORR than for the HPRR.

Furthermore, in the case of the HPRR, one of the contributing factors to the observed deviation from the ideal behaviour can be related to catalysts decomposition or deposition. Indeed, prolonged cycling during CV measurements shows a significant change in shape of the catalytic events (Appendix B4, Figure B.5), followed by increased activity after mixing and saturating the solution with argon, something that was not observed for the ORR. During ORR, the reduction of H_2O_2 is only expected under conditions wherein the overall reduction reaction is nearly mass transport limited in O_2. Under such conditions one would not expect to find a large deviation from the ideal
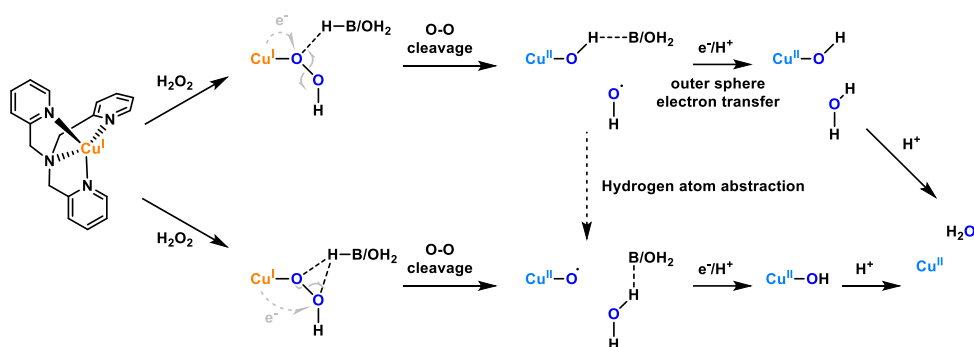
Scheme 3.1. Possible electrocatalytic HPRR pathways in the presence of Cu-tmpa, showing a pathway that proceeds via a Cu hydroxyl and free hydroxyl radical (top), or via copper oxyl radical (bottom). In copper monooxygenases, the possibility of an HAA step has been proposed, enabled by the stabilizing effect of the binding pocket on the hydroxyl radical (see text).

catalytic activity due to catalyst degradation, if one considers that catalyst deactivation is linked to the reduction of H_2O_2 and not to the 2-electron reduction of O_2.

The mechanism for H_2O_2 reduction on copper has been proposed to go through a Fenton-type mechanism, based on research on copper monooxygenases or on bio-inspired copper complexes as monooxygenase mimics.[23-24] In this mechanism, it is proposed that the O-O bond of hydrogen peroxide is split homolytically. This can either result in a copper oxyl radical (Cu-O$^{\bullet-}$) and a free hydroxyl ion (HO$^-$), or a copper hydroxyl species (Cu-OH) and a free hydroxyl radical anion (HO$^{\bullet-}$). For LPMO, it has been found by computational methods that the latter route is more favourable.[56] Additionally, it was shown that the hydroxyl radical was stabilized in the enzyme binding pocket of the active site, preventing damage caused by free radical species. This allowed for a hydrogen atom abstraction (HAA) by the hydroxyl radical from the copper bound hydroxyl group, resulting in Cu-O$^{\bullet-}$ and a water molecule.[24] These possible catalytic pathways are schematically shown in Scheme 3.1, which also includes an outer sphere electron-transfer PCET step as an alternative for the HAA.[57-58] In an electrochemical system, where electron transfer is very fast, and no free radical-stabilizing binding pocket is available, outer sphere electron transfer mediated by the solvent and/or phosphate ions should be considered.

The solvent kinetic isotope effect of 1.4–1.7 for the HPRR catalysed by Cu-tmpa indicates that bond breaking of an O-H bond is involved in the rate-determining step of the catalytic reaction. The relatively low KIE would suggest a weak O-H bond with little covalent character is involved. Solvent KIEs in the same range were observed for an Fe(III)-hydroperoxide porphyrin model for the active site of heme oxygenase.[50-51, 59] Based on computational methods, the solvent KIE was proposed to be associated with

a concerted, stepwise mechanism of proton transfer from the H_2O/H_3O^+ and solvent O-O bond breaking, while involving a rearrangement of the formed hydroxyl radical anion. Such a mechanism would align closer with the top route shown in Scheme 3.1. The resulting free hydroxyl radical anion would also explain the observed instability of the complex under catalytic conditions, as it could react with the tmpa ligand. Further research using hydroxyl radical scavengers would be required to give more insight in whether this is indeed the case.[60]

3.3.   Conclusion

The catalytic performance was investigated of Cu-tmpa for the electrocatalytic reduction of H_2O_2 in pH 7 phosphate buffered neutral aqueous solution. It was confirmed that the reduction of H_2O_2 is significantly slower than O_2 reduction, with rate constants being 10 (TOF_{max}) to 30 (k_{obs}) times lower. As is the case for the ORR, the HPRR displayed a first-order dependence on the catalyst concentration, showing that only a single copper site is involved in the catalytic reaction, which fits well with the reported literature on iron- and copper-catalysed H_2O_2 reduction in enzymes. Additionally, the reaction shows a first-order dependence on the H_2O_2 concentration as well, up until the buffering capacity of the 0.1 M PB buffer is compromised. The effect on the catalytic performance by using D_2O as the solvent was studied, and resulted in a solvent KIE between 1.4–1.7 for the HPRR. However, while this does confirm that a hydrogen or proton transfer is involved in the rate-determining step of the catalytic reaction, the magnitude of the KIE alone does not allow us to pinpoint the exact mechanistic route for the HPRR. Yet, when combining what is known about copper monooxygenases with the obtained solvent KIE and the apparent instability of the Cu-tmpa under catalytic HPRR conditions, the pathway in which free hydroxyl radical anions are formed seems the most likely candidate at this point.

3.4.   Experimental

3.4.1.   General

Aqueous electrolyte solutions were prepared using NaH_2PO_4 (Suprapur®, Merck) and Na_2HPO_4 (Suprapur®, Merck). [Cu(tmpa)(CH_3CN)](OTf)_2 was synthesized as described in Chapter 2. Milli-Q Ultrapure grade water was used for all electrochemical experiments and for the preparation of all aqueous electrolyte solutions. D_2O for the kinetic isotope experiments was obtained from Sigma-Aldrich (99.9 atom% D). H_2O_2 was obtained from Sigma-Aldrich (≥30%, for ultratrace analysis), and the exact concentration was determined via permanganate titration. Alumina suspensions (1.0, 0.3, and 0.05 µm) were obtained from Buehler. pH measurements were done using a Hanna Instruments

HI 4222 pH meter which was calibrated by five-point calibration using IUPAC standard buffers. All gasses used during electrochemical measurements, H_2, O_2, and argon (each 5.0 grade), were supplied by Linde.

3.4.2. Electrochemical measurements

All electrochemical experiments were performed in a custom-built 10 mL single-compartment glass cell with a three-electrode setup. The measurements were performed using Autolab PGSTAT 12, 204, and 128N potentiostats, operated by the Autolab NOVA 2 software. The working electrodes were glassy carbon (GC) disks, either a GC rod (A = 0.071 cm^2, type 1, Alfa Aesar) in hanging meniscus confirmation, or a PEEK encapsulated GC disk (A = 0.071 cm^2, Metrohm) submerged in the solution. Unless otherwise stated, the GC electrodes were manually polished before each catalytic measurement for 5 mins with 1.0, 0.3, and 0.05 µm alumina suspensions on Buehler cloth polishing pads, or with a Struers LaboPol-30 polishing machine using 1.0 µm diamond and 0.04 µm silica suspension on polishing cloths (Dur-type) for 1 min each. This was followed by sonication of the electrode in Milli-Q purified water for 10–15 minutes. A gold wire was used as a counter electrode and was flame annealed and rinsed with Milli-Q purified water. The reference electrode was a reversible hydrogen electrode (RHE) made from a Pt mesh submerged in same electrolyte solution as the main cell compartment, connected via a Luggin capillary, and continuously sparged with H_2 gas. Oxygen-free electrolyte solutions were prepared by saturating the cell for 20 to 30 minutes with Ar, after which an atmosphere of 1 atm Ar was maintained. Oxygen-saturated electrolyte solutions were obtained by saturating the cell for 20 minutes with O_2, after which a 1 atm O_2 atmosphere was maintained.

All glassware was regularly cleaned by submersion in an aqueous oxidizing solution containing 0.5 M H_2SO_4 and 1 mg/mL (6.3 mM) $KMnO_4$ overnight. This is followed by removal of excess $KMnO_4$ and MnO_2 from the glassware with diluted H_2SO_4 and H_2O_2, followed by rinsing the glassware three times with water and boiling twice submerged in Milli-Q purified water.

3.4.3. Electrochemical measurements in D_2O

In preparation of the measurements in D_2O, all glassware was cleaned following the procedure described previously. Additionally, the glassware was dried in an oven at 140 °C for 2 days. The GC working electrode was polished as previously described, followed by sonication in D_2O instead of H_2O. After each polishing cycle and before every measurement, the GC electrode was submerged in the deuterated electrolyte solution for at least 2 minutes. Both the counter and reference electrode were flame annealed and rinsed with D_2O before the experiment. The electrolyte solutions were prepared by

weighing the required phosphate salts (NaH$_2$PO$_4$ and Na$_2$HPO$_4$), which were stored under vacuum in a desiccator containing aluminosilicate drying pearls, in a 100 mL volumetric flask. The volumetric flask was filled to 100 mL with D$_2$O. The apparent pH* was measured using a calibrated pH meter (mentioned in section 3.4.2) filled with non-deuterated electrolyte solution. Both the main cell compartment and the Luggin compartment containing the RHE electrode were filled with the same deuterated PB solution. Catalyst solutions were obtained by first drying Cu-tmpa on a Schlenk-line overnight, before weighing the required amount. This was followed by preparation of concentrated stock solutions of Cu-tmpa (30.0 mM) in D$_2$O for use in the electrochemical experiments. H$_2$O$_2$ (10.0 M in H$_2$O) was used as is, as the maximum proton content during the electrochemical measurements would not exceed 0.01%.

3.5.   References

[1]   G. Grigoropoulou, J. H. Clark, J. A. Elings, *Green Chem.* **2003**, *5*, 1-7.
[2]   R. Noyori, M. Aoki, K. Sato, *Chem. Commun.* **2003**, 1977-1986.
[3]   A. Goti, F. Cardona, in *Green Chemical Reactions* (Eds.: Pietro Tundo, Vittorio Esposito), Springer Netherlands, Dordrecht, **2008**, pp. 191-212.
[4]   A. Podgoršek, M. Zupan, J. Iskra, *Angew. Chem. Int. Ed.* **2009**, *48*, 8424-8450.
[5]   V. Prabhakaran, C. G. Arges, V. Ramani, *Proc. Natl. Acad. Sci.* **2012**, *109*, 1029-1034.
[6]   D. E. Curtin, R. D. Lousenberg, T. J. Henry, P. C. Tangeman, M. E. Tisack, *J. Power Sources* **2004**, *131*, 41-48.
[7]   Y. Wang, K. S. Chen, J. Mishler, S. C. Cho, X. C. Adroher, *Appl. Energy* **2011**, *88*, 981-1007.
[8]   L. An, T. Zhao, X. Yan, X. Zhou, P. Tan, *Sci. Bull.* **2015**, *60*, 55-64.
[9]   K. Asada, *Physiol. Plant.* **1992**, *85*, 235-241.
[10]   E. Nagababu, F. J. Chrest, J. M. Rifkind, *Biochim. Biophys. Acta, Gen. Subj.* **2003**, *1620*, 211-217.
[11]   D. Maiti, A. A. Narducci Sarjeant, K. D. Karlin, *Inorg. Chem.* **2008**, *47*, 8736-8747.
[12]   A. Ghosh, D. A. Mitchell, A. Chanda, A. D. Ryabov, D. L. Popescu, E. C. Upham, G. J. Collins, T. J. Collins, *J. Am. Chem. Soc.* **2008**, *130*, 15116-15126.
[13]   B. J. Day, *Biochem. Pharmacol.* **2009**, *77*, 285-296.
[14]   A. Tovmasyan, et al., *Free Radical Biol. Med.* **2015**, *86*, 308-321.
[15]   S. Signorella, C. Palopoli, G. Ledesma, *Coord. Chem. Rev.* **2018**, *365*, 75-102.
[16]   G. Vaaje-Kolstad, B. Westereng, S. J. Horn, Z. Liu, H. Zhai, M. Sørlie, V. G. H. Eijsink, *Science* **2010**, *330*, 219-222.
[17]   S. J. Horn, G. Vaaje-Kolstad, B. Westereng, V. G. Eijsink, *Biotechnol. Biofuels* **2012**, *5*, 45-45.
[18]   G. Vaaje-Kolstad, Z. Forsberg, J. S. M. Loose, B. Bissaro, V. G. H. Eijsink, *Curr. Opin. Struct. Biol.* **2017**, *44*, 67-76.
[19]   G. R. Hemsworth, E. M. Johnston, G. J. Davies, P. H. Walton, *Trends Biotechnol.* **2015**, *33*, 747-761.
[20]   F. Calderaro, M. Keser, M. Akeroyd, L. E. Bevers, V. G. H. Eijsink, A. Várnai, M. A. van den Berg, *Biotechnol. Biofuels* **2020**, *13*, 195.
[21]   L. Ciano, G. J. Davies, W. B. Tolman, P. H. Walton, *Nat. Catal.* **2018**, *1*, 571-577.
[22]   J. A. Hangasky, M. A. Marletta, *Biochemistry* **2018**, *57*, 3191-3199.
[23]   S. Kim, J. W. Ginsbach, J. Y. Lee, R. L. Peterson, J. J. Liu, M. A. Siegler, A. A. Sarjeant, E. I. Solomon, K. D. Karlin, *J. Am. Chem. Soc.* **2015**, *137*, 2867-2874.
[24]   B. Wang, P. H. Walton, C. Rovira, *ACS Catal.* **2019**, *9*, 4958-4969.
[25]   R. L. Lieberman, A. C. Rosenzweig, *Nature* **2005**, *434*, 177-182.
[26]   R. A. Himes, K. D. Karlin, *Curr. Opin. Chem. Biol.* **2009**, *13*, 119-131.
[27]   S. M. Smith, S. Rawat, J. Telser, B. M. Hoffman, T. L. Stemmler, A. C. Rosenzweig, *Biochemistry* **2011**, *50*, 10231-10240.

[28]   L. Cao, O. Caldararu, A. C. Rosenzweig, U. Ryde, *Angew. Chem. Int. Ed.* **2018**, *57*, 162-166.
[29]   M. Miyanishi, T. Abe, Y. Hori, Y. Shiota, K. Yoshizawa, *Inorg. Chem.* **2019**, *58*, 12280-12288.
[30]   M. O. Ross, F. MacMillan, J. Wang, A. Nisthal, T. J. Lawton, B. D. Olafson, S. L. Mayo, A. C. Rosenzweig, B. M. Hoffman, *Science* **2019**, *364*, 566-570.
[31]   W. Liu, D. Zuckerbrod, *J. Electrochem. Soc.* **2005**, *152*, A1165.
[32]   T. Kinumoto, M. Inaba, Y. Nakayama, K. Ogata, R. Umebayashi, A. Tasaka, Y. Iriyama, T. Abe, Z. Ogumi, *J. Power Sources* **2006**, *158*, 1222-1228.
[33]   M. Inaba, T. Kinumoto, M. Kiriake, R. Umebayashi, A. Tasaka, Z. Ogumi, *Electrochim. Acta* **2006**, *51*, 5746-5753.
[34]   K. Hongsirikarn, X. Mo, J. G. Goodwin, S. Creager, *J. Power Sources* **2011**, *196*, 3060-3072.
[35]   S. Fukuzumi, Y. Yamada, K. D. Karlin, *Electrochim. Acta* **2012**, *82*, 493-511.
[36]   L. An, T. S. Zhao, X. L. Zhou, L. Wei, X. H. Yan, *RSC Adv.* **2014**, *4*, 65031-65034.
[37]   E. Miglbauer, P. J. Wójcik, E. D. Głowacki, *Chem. Commun.* **2018**, *54*, 11873-11876.
[38]   Y. Yang, Y. Xue, F. Huang, H. Zhang, K. Tao, R. Zhang, Q. Shen, H. Chang, *ACS Appl. Energy Mater.* **2018**, *1*, 5328-5335.
[39]   J. M. Campos-Martin, G. Blanco-Brieva, J. L. G. Fierro, *Angew. Chem. Int. Ed.* **2006**, *45*, 6962-6984.
[40]   R. Hage, A. Lienke, *Angew. Chem. Int. Ed.* **2006**, *45*, 206-222.
[41]   S. A. M. van Stroe-Biezen, F. M. Everaerts, L. J. J. Janssen, R. A. Tacken, *Anal. Chim. Acta* **1993**, *273*, 553-560.
[42]   S. B. Hall, E. A. Khudaish, A. L. Hart, *Electrochim. Acta* **1999**, *44*, 2455-2462.
[43]   K. Aoki, M. Ishida, K. Tokuda, K. Hasebe, *J. Electroanal. Chem.* **1988**, *251*, 63-71.
[44]   P. Westbroek, E. Temmerman, *J. Electroanal. Chem.* **2000**, *482*, 40-47.
[45]   A. Krężel, W. Bal, *J. Inorg. Biochem.* **2004**, *98*, 161-166.
[46]   M. M. Ghoneim, S. Clouser, E. Yeager, *J. Electrochem. Soc.* **1985**, *132*, 1160-1162.
[47]   J. Xu, W. Huang, R. L. McCreery, *J. Electroanal. Chem.* **1996**, *410*, 235-242.
[48]   M. Langerman, D. G. H. Hetterscheid, *Angew. Chem. Int. Ed.* **2019**, *58*, 12974-12978.
[49]   E. Gopinath, T. C. Bruice, *J. Am. Chem. Soc.* **1991**, *113*, 4657-4665.
[50]   R. Davydov, T. Matsui, H. Fujii, M. Ikeda-Saito, B. M. Hoffman, *J. Am. Chem. Soc.* **2003**, *125*, 16208-16209.
[51]   D. Kumar, S. P. de Visser, S. Shaik, *J. Am. Chem. Soc.* **2005**, *127*, 8204-8213.
[52]   C. Costentin, S. Drouet, M. Robert, J.-M. Savéant, *J. Am. Chem. Soc.* **2012**, *134*, 11235-11242.
[53]   D. J. Wasylenko, C. Rodríguez, M. L. Pegis, J. M. Mayer, *J. Am. Chem. Soc.* **2014**, *136*, 12544-12547.
[54]   C. Costentin, J.-M. Savéant, *ChemElectroChem* **2014**, *1*, 1226-1236.
[55]   E. S. Rountree, B. D. McCarthy, T. T. Eisenhart, J. L. Dempsey, *Inorg. Chem.* **2014**, *53*, 9983-10002.
[56]   B. Wang, E. M. Johnston, P. Li, S. Shaik, G. J. Davies, P. H. Walton, C. Rovira, *ACS Catal.* **2018**, *8*, 1346-1351.
[57]   N. Ramaswamy, S. Mukerjee, *J. Phys. Chem. C* **2011**, *115*, 18015-18026.
[58]   I. Kenkel, et al., *J. Am. Chem. Soc.* **2017**, *139*, 1472-1484.
[59]   P. K. Sharma, R. Kevorkiants, S. P. de Visser, D. Kumar, S. Shaik, *Angew. Chem. Int. Ed.* **2004**, *43*, 1129-1132.
[60]   A. C. Maier, E. H. Iglebaek, M. Jonsson, *ChemCatChem* **2019**, *11*, 5435-5438.